Properties of Neutron Star Crusts with Accurately Calibrated Nuclear Energy Density Functionals

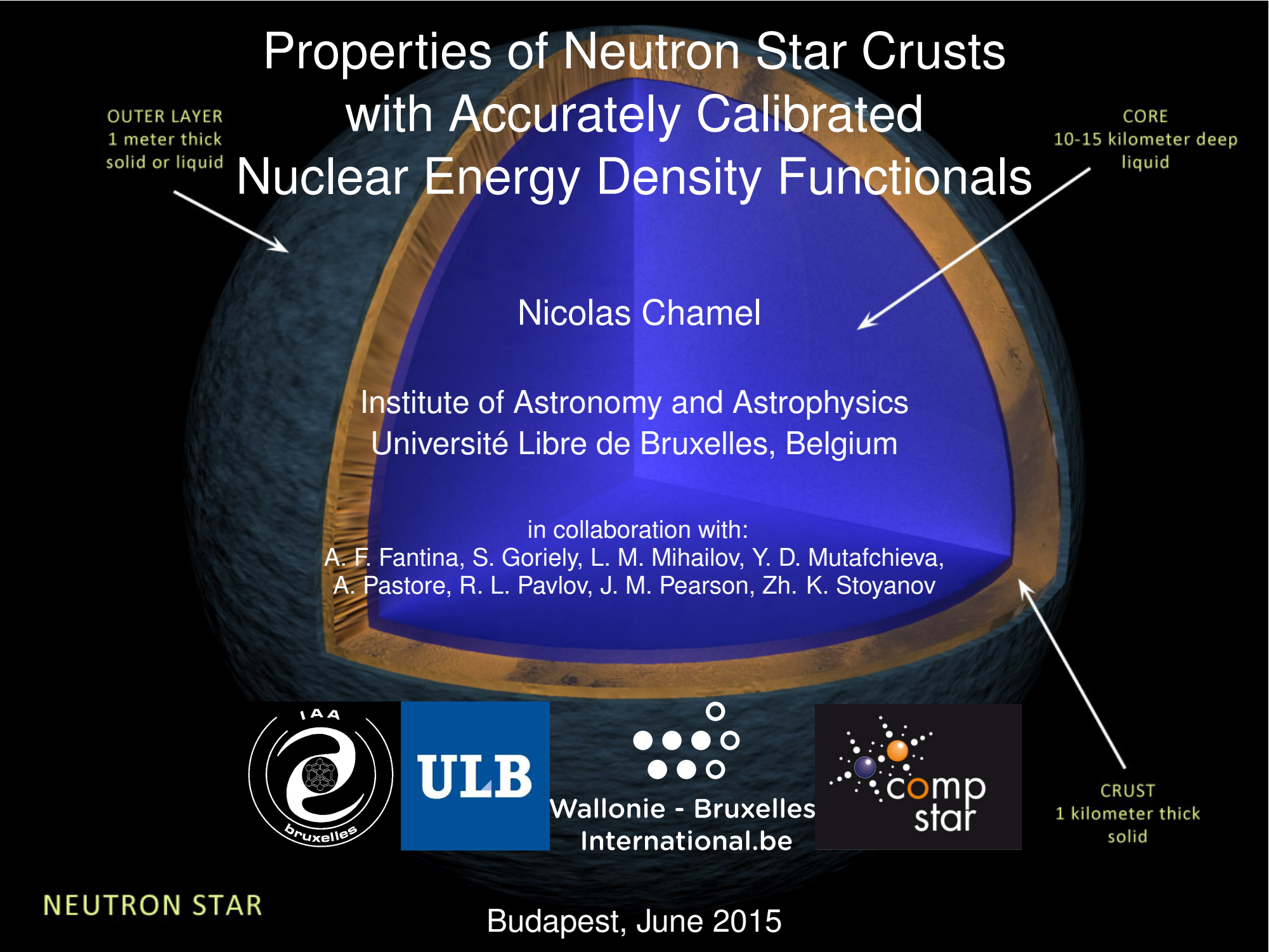

Nicolas Chamel

Institute of Astronomy and Astrophysics
Université Libre de Bruxelles, Belgium

in collaboration with:
A. F. Fantina, S. Goriely, L. M. Mihailov, Y. D. Mutafchieva,
A. Pastore, R. L. Pavlov, J. M. Pearson, Zh. K. Stoyanov

Budapest, June 2015

Punchline

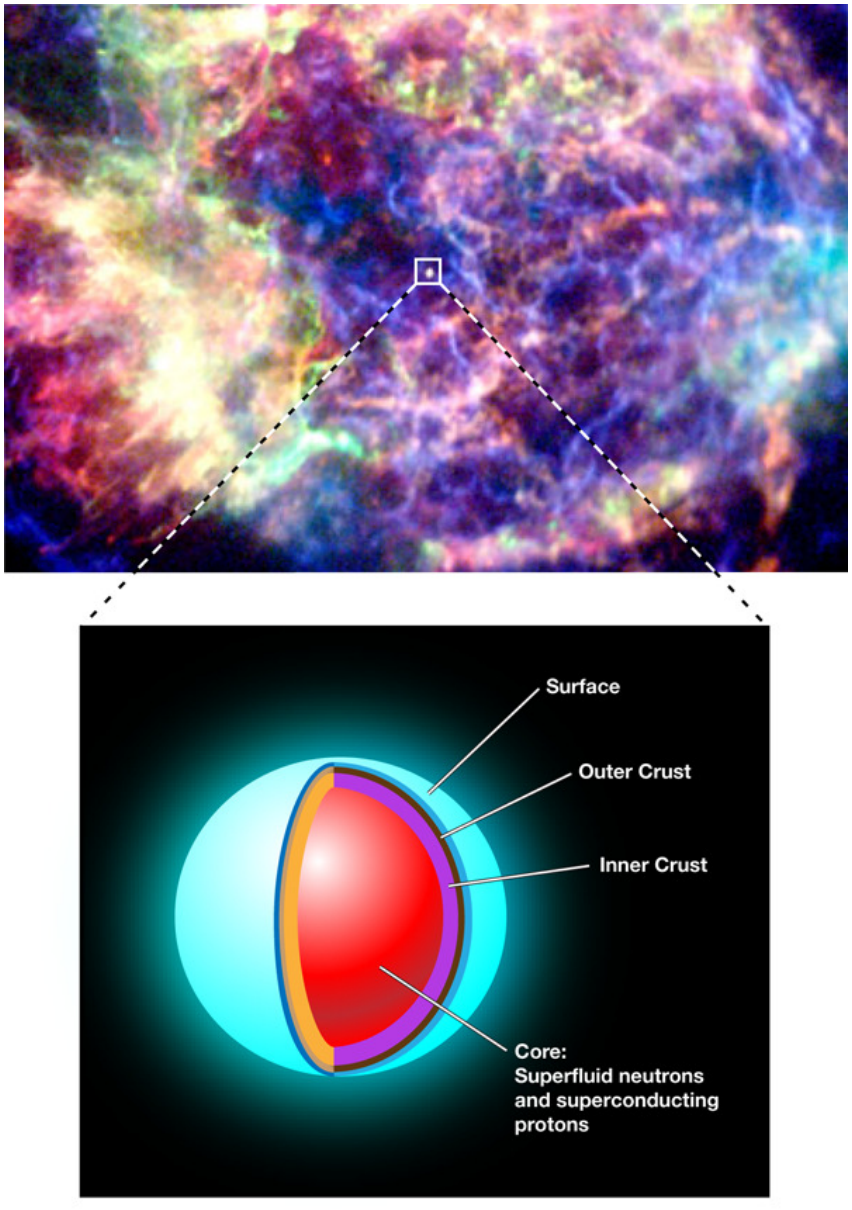

Even though the crust of a neutron star represents about $\sim 1\%$ of the stellar mass and $\sim 10\%$ of the stellar radius, it is thought to be related to various observed phenomena:

- pulsar glitches,
- X-ray bursts and superbursts,
- deep crustal heating,
- thermal relaxation in SXT,
- QPOs in SGR, etc.

Our goal is to construct realistic models of neutron-star crusts using the nuclear energy density functional theory.

Nuclear Energy Density Functional Theory

What is it all about?

The energy $E\Big[n_q(\boldsymbol{r}), \boldsymbol{\nabla} n_q(\boldsymbol{r}), \tau_q(\boldsymbol{r}), \boldsymbol{J_q}(\boldsymbol{r})\Big]$ can be expressed as a *functional* of various densities and currents ($q = n, p$):

$$n_q(\boldsymbol{r}) = \sum_{k,\sigma=\uparrow,\downarrow} |\varphi^{(q)}_{k\sigma}(\boldsymbol{r})|^2, \qquad \tau_q(\boldsymbol{r}) = \sum_{k,\sigma=\uparrow,\downarrow} |\boldsymbol{\nabla}\varphi^{(q)}_{k\sigma}(\boldsymbol{r})|^2$$

$$\boldsymbol{J_q}(\boldsymbol{r}) = \frac{\mathrm{i}}{2} \sum_{k,\sigma,\sigma'=\uparrow,\downarrow} \left\{ \varphi^{(q)}_{k\sigma}(\boldsymbol{r}) \boldsymbol{\nabla} \varphi^{(q)}_{k\sigma'}(\boldsymbol{r})^* - \varphi^{(q)}_{k\sigma'}(\boldsymbol{r})^* \boldsymbol{\nabla} \varphi^{(q)}_{k\sigma}(\boldsymbol{r}) \right\} \times \langle \sigma' | \hat{\boldsymbol{\sigma}} | \sigma \rangle$$

The single-particle wavefunctions $\varphi^{(q)}_{k\sigma}(\boldsymbol{r})$ are obtained from the *self-consistent* "Hartree-Fock" (HF) equations:

$$\left[-\boldsymbol{\nabla} \cdot \frac{\hbar^2}{2M^\star_q(\boldsymbol{r})} \boldsymbol{\nabla} + U_q(\boldsymbol{r}) - \mathrm{i} \boldsymbol{W_q}(\boldsymbol{r}) \cdot \boldsymbol{\nabla} \times \boldsymbol{\sigma} \right] \varphi^{(q)}(\boldsymbol{r}) = \varepsilon^{(q)} \varphi^{(q)}(\boldsymbol{r})$$

$$\frac{\hbar^2}{2M^\star_q(\boldsymbol{r})} \equiv \frac{\delta E}{\delta \tau_q(\boldsymbol{r})}, \qquad U_q(\boldsymbol{r}) \equiv \frac{\delta E}{\delta n_q(\boldsymbol{r})}, \qquad \boldsymbol{W_q}(\boldsymbol{r}) \equiv \frac{\delta E}{\delta \boldsymbol{J_q}(\boldsymbol{r})}.$$

This scheme can be extended to account for nuclear pairing: Hartree-Fock-Bogoliubov (HFB) equations.

Problem: we don't know what the exact functional is... We have thus to rely on phenomenological functionals.

Which functional should we choose?

The nuclear energy density functional theory has been very successfully applied to describe the structure and the dynamics of medium-mass and heavy nuclei.

However, most functionals are not suitable for astrophysical applications:

- they were adjusted to a few selected nuclei (mostly in the stability valley)
- they yield unrealistic neutron-matter equation of state
- they yield unrealistic pairing gaps in nuclear matter
- they yield unrealistic effective masses
- they lead to spurious instabilities in nuclear matter (e.g. ferromagnetic transition).

Brussels-Montreal Skyrme functionals (BSk)

These functionals were fitted to both experimental data and N-body calculations using realistic forces.

Experimental data:

- all atomic masses with $Z, N \geq 8$ from the Atomic Mass Evaluation (root-mean square deviation: 0.5-0.6 MeV)
  `http://www.astro.ulb.ac.be/bruslib/`
- charge radii
- incompressibility $K_v = 240 \pm 10$ MeV (ISGMR)
  Colò et al., Phys.Rev.C70, 024307 (2004).

N-body calculations using realistic forces:

- equation of state of pure neutron matter
- ${}^1S_0$ pairing gaps in nuclear matter
- effective masses in nuclear matter

Phenomenological corrections for atomic nuclei

For atomic nuclei, we add the following corrections:

- Wigner energy

$$E_W = V_W \exp\left\{ -\lambda \left(\frac{N-Z}{A} \right)^2 \right\} + V'_W |N-Z| \exp\left\{ -\left(\frac{A}{A_0} \right)^2 \right\}$$

  $V_W \sim -2$ MeV, $V'_W \sim 1$ MeV, $\lambda \sim 300$ MeV, $A_0 \sim 20$

- rotational and vibrational spurious collective energy

$$E_{\text{coll}} = E_{\text{rot}}^{\text{crank}} \left\{ b \ \tanh(c|\beta_2|) + d|\beta_2| \ \exp\{-I(|\beta_2| - \beta_2^0)^2\} \right\}$$

This latter correction was shown to be in good agreement with more elaborate calculations (5D collective Hamiltonian).
Goriely, Chamel, Pearson, Phys.Rev.C82,035804(2010).

In this way, these collective effects do not contaminate the parameters (≤ 20) of the functional.

Brussels-Montreal Skyrme functionals

Main features of the latest functionals:

- **fit to realistic $^1S_0$ pairing gaps** in symmetric and neutron matter (BSk16-17)
  Chamel, Goriely, Pearson, Nucl.Phys.A812,72 (2008)
  Goriely, Chamel, Pearson, PRL102,152503 (2009).
- **removal of spurious spin and spin-isospin instabilities** in nuclear matter (BSk18)
  Chamel, Goriely, Pearson, Phys.Rev.C80,065804(2009)
- **fit to realistic neutron-matter equation of state** (BSk19-21)
  Goriely, Chamel, Pearson, Phys.Rev.C82,035804(2010)
- **fit to different symmetry energies** (BSk22-26)
  Goriely, Chamel, Pearson, Phys.Rev.C88,024308(2013)
- **optimal fit of the 2012 AME** - rms 0.512 MeV (BSk27*)
  Goriely, Chamel, Pearson, Phys.Rev.C88,061302(R)(2013)
- **generalized spin-orbit coupling** (BSk28-29)
  Goriely, Nucl.Phys.A933,68(2015).

Microscopic Models of Neutron Star Crusts

Description of neutron star crust below neutron drip

Main assumptions:

- atoms are fully pressure ionized $\rho \gg 10AZ$ g cm^{-3}
- the crust is a solid crystal

  $T < T_m \approx 1.3 \times 10^5 Z^2 \left(\frac{\rho_6}{A}\right)^{1/3}$ K $\qquad \rho_6 \equiv \rho/10^6$ g cm^{-3}
- electrons are uniformly distributed and are highly degenerate

  $T < T_F \approx 5.93 \times 10^9 (\gamma_r - 1)$ K

  $\gamma_r \equiv \sqrt{1 + x_r^2}\,, \qquad x_r \equiv \frac{p_F}{m_e c} \approx 1.00884 \left(\frac{\rho_6 Z}{A}\right)^{1/3}$
- matter is fully catalyzed

The only microscopic inputs are nuclear masses. We have made use of the experimental data (Atomic Mass Evaluation) complemented with our HFB mass tables.

Pearson,Goriely,Chamel,Phys.Rev.C83,065810(2011).

Composition of the outer crust of a neutron star

The composition of the crust is completely determined by experimental nuclear masses down to about 200m for a $1.4 M_{\odot}$ neutron star with a 10 km radius

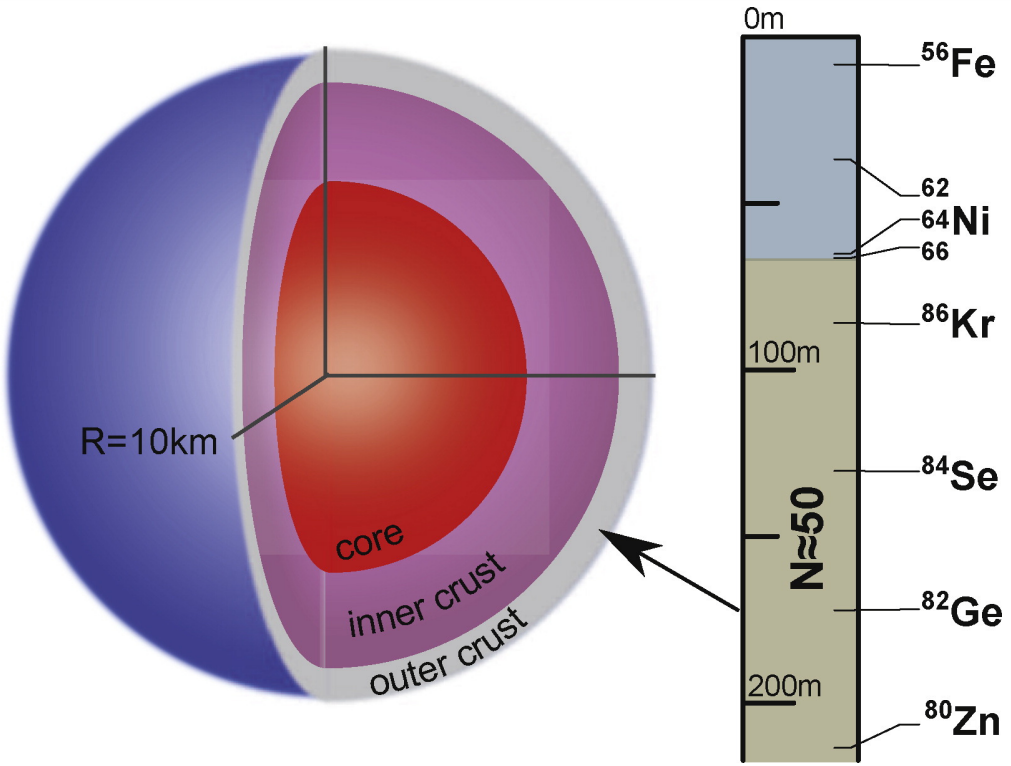

Roca-Maza, Piekarewicz, Phys.Rev.C78,025807(2008)
Pearson,Goriely,Chamel,Phys.Rev.C83,065810(2011)
Kreim, Hempel, Lunney, Schaffner-Bielich, Int.J.M.Spec.349-350,63(2013)

Plumbing neutron stars to new depths

New precision measurements of the mass of short-lived zinc nuclides by the ISOLTRAP collaboration at CERN's ISOLDE radioactive-beam facility has recently allowed to "drill" deeper into the crust.

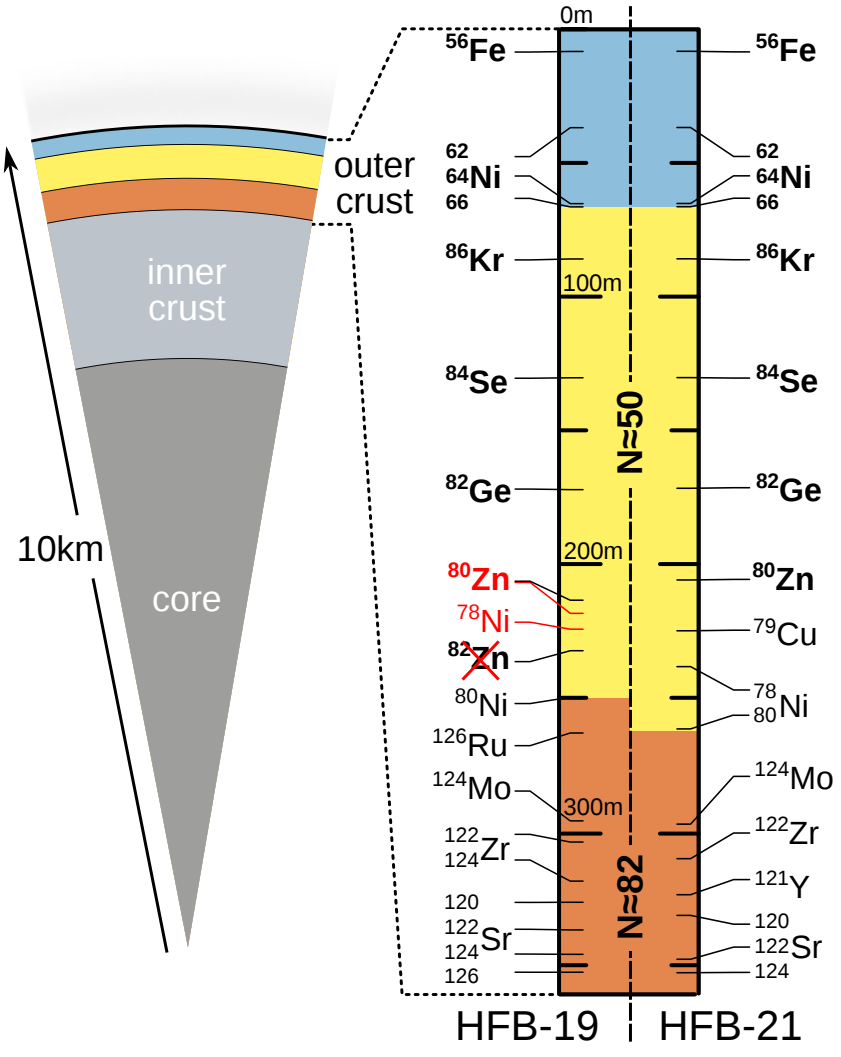

Wolf et al.,PRL110,041101(2013).

Composition of the outer crust of a nonaccreting neutron star (catalyzed matter)

Deeper in the star, the composition is model-dependent:

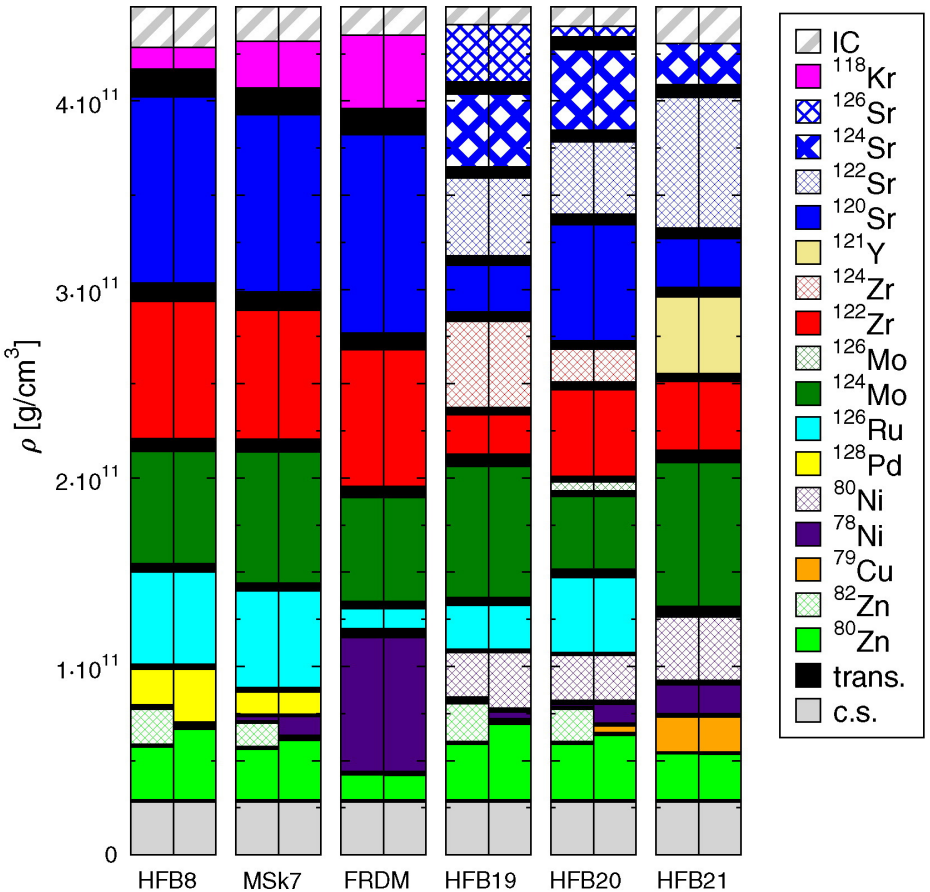

Kreim, Hempel, Lunney, Schaffner-Bielich, Int.J.M.Spec.349-350,63(2013)

Impact of a strong magnetic field on the composition of the crust?

In a strong magnetic field $\vec{B}$ (along let's say the z-axis), the **electron motion perpendicular to the field is quantized**:

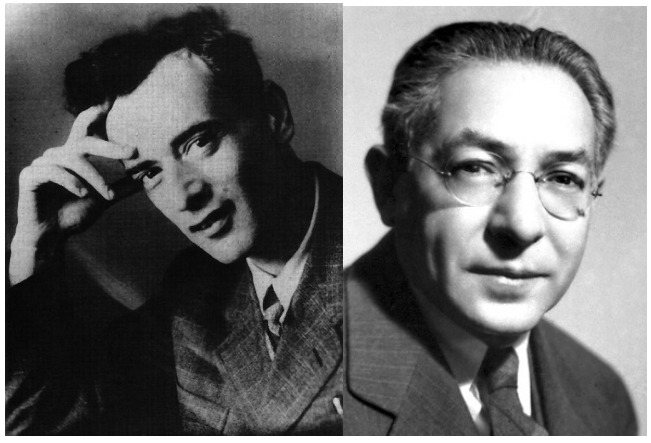

Landau-Rabi levels

Rabi, Z.Phys.49, 507 (1928).

$$e_\nu = \sqrt{c^2 p_z^2 + m_e^2 c^4 (1 + 2\nu B_\star)}$$

where $\nu = 0, 1, ...$ and $B_\star = B/B_c$

with $B_c = \dfrac{m_e^2 c^3}{\hbar e} \simeq 4.4 \times 10^{13}$ G.

Maximum number of occupied Landau levels for HFB-21:

$B_\star$	1500	1000	500	100	50	10	1
$\nu_{\max}$	1	2	3	14	28	137	1365

Only $\nu = 0$ is filled for $\rho < 2.07 \times 10^6 \left(\dfrac{A}{Z}\right) B_\star^{3/2}$ g cm^{-3}.

Landau quantization can change the composition of the crust.

Composition of the outer crust of a magnetar

Sequence of nuclides for HFB-21 and $B_\star \equiv B/(4.4 \times 10^{13}\ \mathrm{G})$:

$B_\star = 0$	$B_\star = 1$	$B_\star = 10$	$B_\star = 100$	$B_\star = 1000$	$B_\star = 2000$
^{56}**Fe**	^{56}**Fe**	^{56}**Fe**	^{56}**Fe**	^{56}**Fe**	^{56}**Fe**
^{62}**Ni**	^{62}**Ni**	^{62}**Ni**	^{62}**Ni**	^{62}**Ni**	^{62}**Ni**
^{58}**Fe**	^{58}**Fe**	–	–	–	–
^{64}**Ni**	^{64}**Ni**	^{64}**Ni**	^{64}**Ni**	^{64}**Ni**	–
^{66}**Ni**	^{66}**Ni**	^{66}**Ni**	–	–	–
–	–	–	–	^{88}**Sr**	^{88}**Sr**
^{86}**Kr**	^{86}**Kr**	^{86}**Kr**	^{86}**Kr**	^{86}**Kr**	^{86}**Kr**
^{84}**Se**	^{84}**Se**	^{84}**Se**	^{84}**Se**	^{84}**Se**	^{84}**Se**
^{82}**Ge**	^{82}**Ge**	^{82}**Ge**	^{82}**Ge**	^{82}**Ge**	^{82}**Ge**
–	–	–	–	–	^{132}**Sn**
^{80}**Zn**	^{80}**Zn**	^{80}**Zn**	^{80}**Zn**	^{80}**Zn**	^{80}**Zn**
–	–	–	–	–	^{130}**Cd**
–	–	–	–	–	^{128}Pd
–	–	–	–	–	^{126}Ru
^{79}Cu	^{79}Cu	^{79}Cu	^{79}Cu	^{79}Cu	–
^{78}Ni	^{78}Ni	^{78}Ni	^{78}Ni	^{78}Ni	–
^{80}Ni	^{80}Ni	^{80}Ni	^{80}Ni	^{80}Ni	–
^{124}Mo	^{124}Mo	^{124}Mo	^{124}Mo	^{124}Mo	^{124}Mo
^{122}Zr	^{122}Zr	^{122}Zr	^{122}Zr	^{122}Zr	^{122}Zr
^{121}Y	^{121}Y	^{121}Y	^{121}Y	^{121}Y	^{121}Y
^{120}Sr	^{120}Sr	^{120}Sr	^{120}Sr	^{120}Sr	^{120}Sr
^{122}Sr	^{122}Sr	^{122}Sr	^{122}Sr	^{122}Sr	^{122}Sr
^{124}Sr	^{124}Sr	^{124}Sr	^{124}Sr	^{124}Sr	^{124}Sr

Chamel et al.,Phys.Rev.C86, 055804(2012).

Equation of state of the outer crust of magnetars

Matter in a magnetar is much more incompressible and less neutron-rich than in a neutron star.

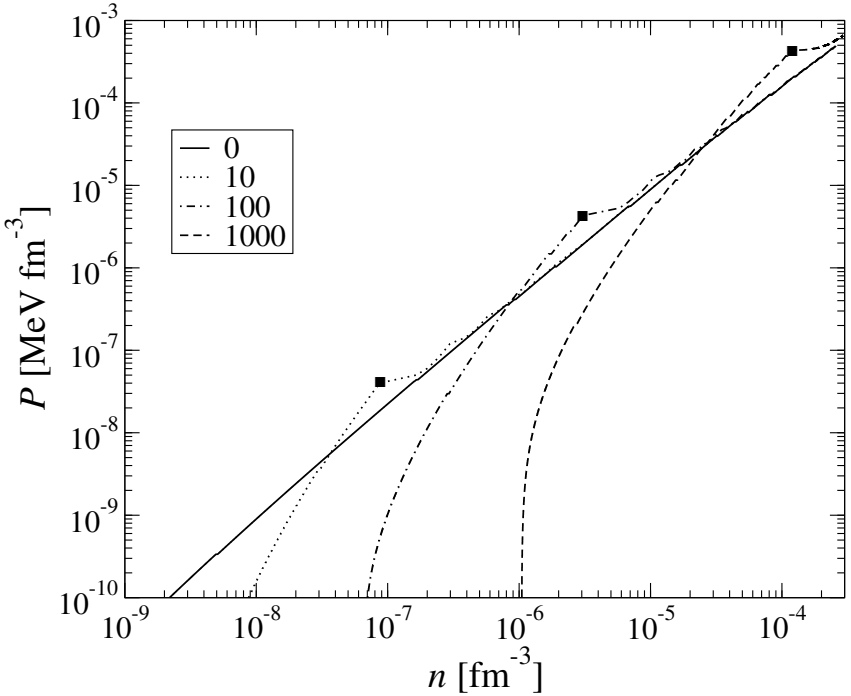

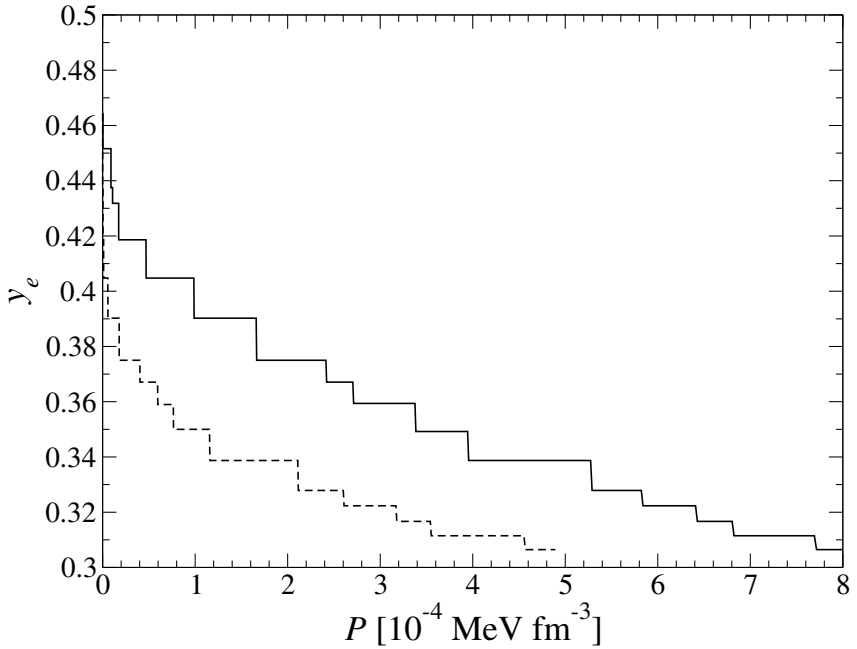

$$P \approx P_0 \left(\frac{n}{n_s} - 1 \right)^2$$

$$y_e \approx \frac{1}{2} \left(1 - \sqrt{\frac{\pi^2 \lambda_e^3 m_e c^2 P}{4 B_\star J^2}} \right)$$

Chamel et al.,Phys.Rev.C86, 055804(2012).

Neutron-drip transition: general considerations

With increasing pressure, nuclei become progressively more neutron rich until neutrons start to drip out.

At this point, nuclei are actually stable against neutron emission but are unstable against *electron captures* accompanied by neutron emission ${}^{A}_{Z}\mathrm{X} + \Delta Z e^{-} \rightarrow {}^{A-\Delta N}_{Z-\Delta Z}\mathrm{Y} + \Delta N\, n + \Delta Z\, \nu_e$

- **nonaccreting neutron stars**
  According to the cold catalyzed matter hypothesis, all kinds of reactions are allowed: the ground state is reached for $\Delta Z = Z$ and $\Delta N = A$.
- **accreting neutron stars**
  Multiple electron captures are very unlikely therefore $\Delta Z = 1$ ($\Delta N \geq 1$). The dripping nucleus ${}^{A}_{Z}\mathrm{X}$ is such that ${}^{A}_{Z-1}\mathrm{Y}$ is unstable against neutron emission.

ρ_{drip} and P_{drip} can be expressed by simple analytical formulas.
Chamel, Fantina, Zdunik, Haensel, Phys. Rev. C91,055803(2015).

Neutron-drip transition in unmagnetized neutron stars

- **nonaccreting neutron stars**

	outer crust	drip line	$\rho_{\rm drip}$ (g cm^{-3})	$P_{\rm drip}$ (dyn cm^{-2})
HFB-19	^{126}Sr (0.73)	^{121}Sr (-0.62)	4.40×10^{11}	7.91×10^{29}
HFB-20	^{126}Sr (0.48)	^{121}Sr (-0.71)	4.39×10^{11}	7.89×10^{29}
HFB-21	^{124}Sr (0.83)	^{121}Sr (-0.33)	4.30×10^{11}	7.84×10^{29}

- **accreting neutron stars**

With HFB-21:

A	Z	ΔN	$\rho_{\rm drip-acc}$ (10^{11} g cm^{-3})	$P_{\rm drip-acc}$ (10^{29} dyn cm^{-2})
104	32	1	4.85	9.31
105	33	1	3.42	6.01
68	22	1	4.13	8.12
64	20	3	5.84	12.3
72	22	1	5.35	10.6
76	24	1	5.02	10.2
98	32	1	3.42	6.33
103	33	1	2.83	4.79
106	34	1	3.65	6.72
66	22	1	3.58	6.98
64	20	3	5.84	12.3
60	20	1	3.36	6.43

Neutron drip transition in magnetars

The neutron drip pressure increases with B whereas the composition of matter remains the same.

In the strongly quantizing regime, $\mu_e^{\rm drip} = \dfrac{-M(A,Z)c^2 + Am_nc^2}{Z}$

$$P_{\rm drip} \approx \frac{B_\star \mu_e^{\rm drip\,2}}{4\pi^2\lambda_e^3 m_e c^2}\left[1 - \frac{1}{3}C\alpha Z^{2/3}\left(\frac{4B_\star}{\pi^2}\right)^{1/3}\left(\frac{m_e c^2}{\mu_e^{\rm drip}}\right)^{2/3}\right]$$

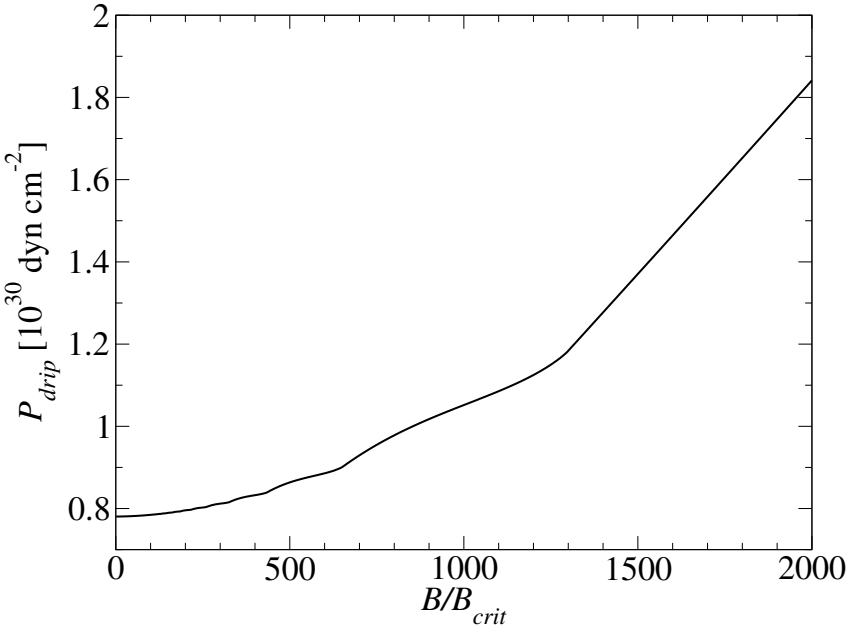

Example using HFB-24 and $C = -1.44423$ (bcc lattice).

We find that the dripping nucleus is $^{124}_{38}$Sr independently of B.

$\mu_e^{\rm drip} \approx 24.81$ MeV.

Chamel et al.,Phys.Rev.C91, 065801(2015).

Neutron drip transition in magnetars

The neutron drip density exhibits typical quantum oscillations.

Example using HFB-24:

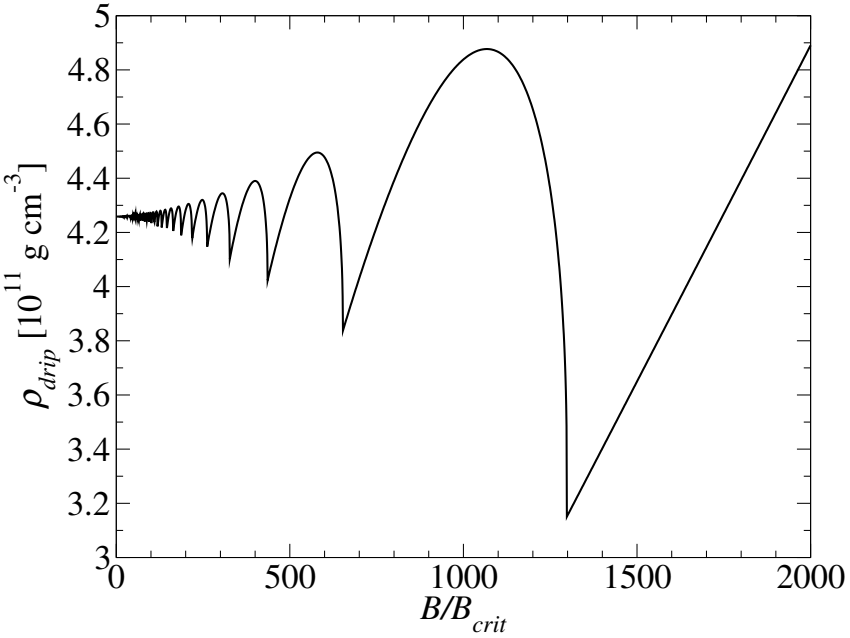

These oscillations are almost universal:

$$\frac{\rho_{\rm drip}^{\rm min}}{\rho_{\rm drip}(B_\star = 0)} \approx \frac{3}{4}$$

$$\frac{\rho_{\rm drip}^{\rm max}}{\rho_{\rm drip}(B_\star = 0)} \approx \frac{35 + 13\sqrt{13}}{72}$$

In the strongly quantizing regime,

$$\rho_{\rm drip} \approx \frac{A}{Z} m \frac{\mu_e^{\rm drip}}{m_e c^2} \frac{B_\star}{2\pi^2 \lambda_e^3} \left[1 - \frac{4}{3} C \alpha Z^{2/3} \left(\frac{B_\star}{2\pi^2} \right)^{1/3} \left(\frac{m_e c^2}{\mu_e^{\rm drip}} \right)^{2/3} \right]$$

Chamel et al.,Phys.Rev.C91, 065801(2015).

Description of neutron star crust beyond neutron drip

Extended Thomas-Fermi+Strutinsky Integral (ETFSI) approach:

- $\tau_q(\boldsymbol{r})$ and $\boldsymbol{J_q}(\boldsymbol{r})$ are expanded into $n_q(\boldsymbol{r})$ and its gradients
- minimization of the energy yields
  $\lambda_q = \dfrac{\delta E}{\delta n_q(r)}$ whose solutions are $\widetilde{n_q}(\boldsymbol{r})$ and $E[\widetilde{n_q}(\boldsymbol{r})] = E_{\rm ETF}$
- shell effects are added perturbatively using the Strutinsky integral theorem $E \approx E_{\rm ETF} + \delta E_n + \delta E_p$

$$\delta E_q = \sum_k \widetilde{\varepsilon}_k^{(q)} - \int d^3\boldsymbol{r} \left\{ \frac{\hbar^2}{2\widetilde{M_q}^\star(\boldsymbol{r})} \widetilde{\tau}_q(\boldsymbol{r}) + \widetilde{n_q}(\boldsymbol{r}) \widetilde{U_q}(\boldsymbol{r}) + \widetilde{\boldsymbol{J_q}}(\boldsymbol{r}) \cdot \widetilde{\boldsymbol{W_q}}(\boldsymbol{r}) \right\}$$

$$\left\{ -\boldsymbol{\nabla} \cdot \frac{\hbar^2}{2\widetilde{M_q}^\star(\boldsymbol{r})} \boldsymbol{\nabla} + \widetilde{U_q}(\boldsymbol{r}) - \mathrm{i}\widetilde{\boldsymbol{W_q}}(\boldsymbol{r}) \cdot \boldsymbol{\nabla} \times \boldsymbol{\sigma} \right\} \varphi_k^{(q)}(\boldsymbol{r}) = \widetilde{\varepsilon}_k^{(q)} \varphi_k^{(q)}(\boldsymbol{r})$$

Advantages of the ETFSI method:

- very fast approximation to the full HF equations (the same scheme can be extended to pairing)
- avoids the difficulties related to boundary conditions
  Chamel et al.,Phys.Rev.C75(2007),055806.

Description of neutron star crust beyond neutron drip

In order to further speed-up the calculations, we make the following approximations:

- neutron-proton clusters are spherical and $n_q(\boldsymbol{r})$ are parametrized as $n_q(r) = n_{Bq} + n_{\Lambda q} f_q(r)$, where
$$f_q(r) = \frac{1}{1 + \exp\left\{\left(\frac{C_q - R}{r - R}\right)^2 - 1\right\} \exp\left(\frac{r - C_q}{a_q}\right)}$$
- the Wigner-Seitz approximation is used to compute the lattice energy,
- neutron shell effects are neglected ($\delta E_n \ll \delta E_p$),
- electrons are uniformly distributed.

Pearson,Chamel,Goriely,Ducoin,Phys.Rev.C85,065803(2012).
Onsi,Dutta,Chatri,Goriely,Chamel,Pearson, Phys.Rev.C77,065805 (2008).

Structure of nonaccreting neutron star crusts

With increasing density, the clusters keep essentially the same size but become more and more dilute.

The crust-core transition predicted by the ETFSI method agrees very well with the instability analysis of homogeneous nuclear matter.

	$\bar{n}_{cc}$ (fm^{-3})	P_{cc} (MeV fm^{-3})
BSk27*	0.0919	0.439
BSk21	0.0809	0.268
BSk20	0.0854	0.365
BSk19	0.0885	0.428
SLy4	0.0798	0.361

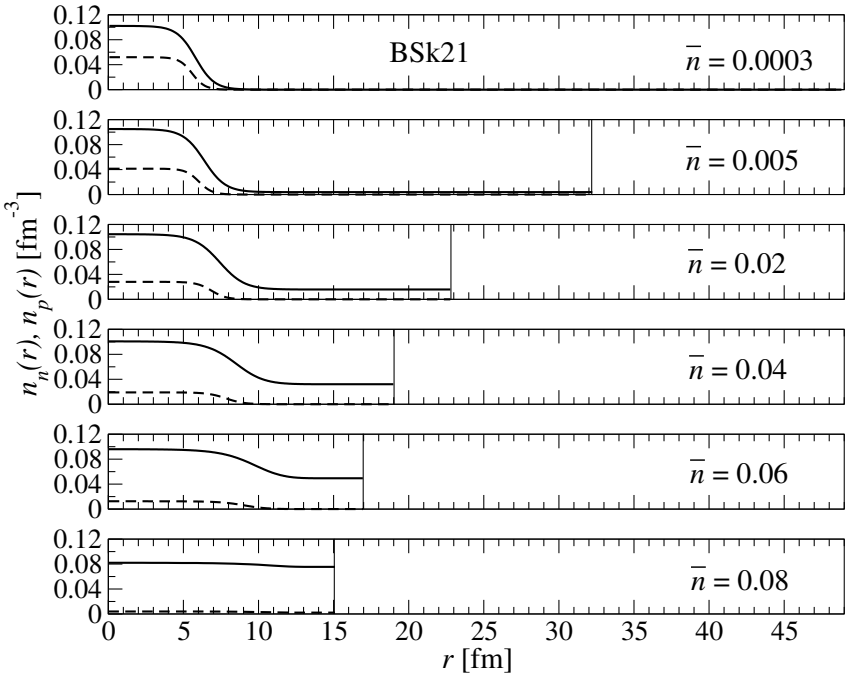

Chamel et al., Acta Phys. Pol.46,349(2015).
Pearson,Chamel,Goriely,Ducoin,Phys.Rev.C85,065803(2012).

The crust-core transition is of very weak first order.

Matching between outer and inner crusts

Comparison of inner- and outer-crust codes at drip point; results for latter code in parentheses. e is the internal energy per nucleon, and P the pressure.

	$\bar{n}_{\rm drip}$ (fm^{-3})	Z	N	e (MeV)	P (10^{-4} MeV fm^{-3})
BSk19	2.63×10^{-4}	40 (38)	96 (88)	-1.79 (-1.87)	5.1 (4.9)
BSk20	2.63×10^{-4}	40 (38)	95 (88)	-1.79 (-1.87)	5.1 (4.9)
BSk21	2.57×10^{-4}	40 (38)	94 (86)	-1.82 (-1.90)	5.0 (4.9)
SLy4	2.46×10^{-4}	40 (38)	93 (82)	-1.79 (-1.96)	4.7 (4.8)

The few % discrepancies can be attributed to

- the neglect of pairing,
- the neglect of neutron shell effects,
- the parametrized density distributions,
- the neglect of rotational and vibrational corrections.

Composition of the inner crust of a nonaccreting neutron star: ETF vs ETFSI

- The ordinary nuclear shell structure seems to be preserved apart from $Z = 40$ (quenched spin-orbit?).
- The energy differences between different configurations become very small as the density increases!

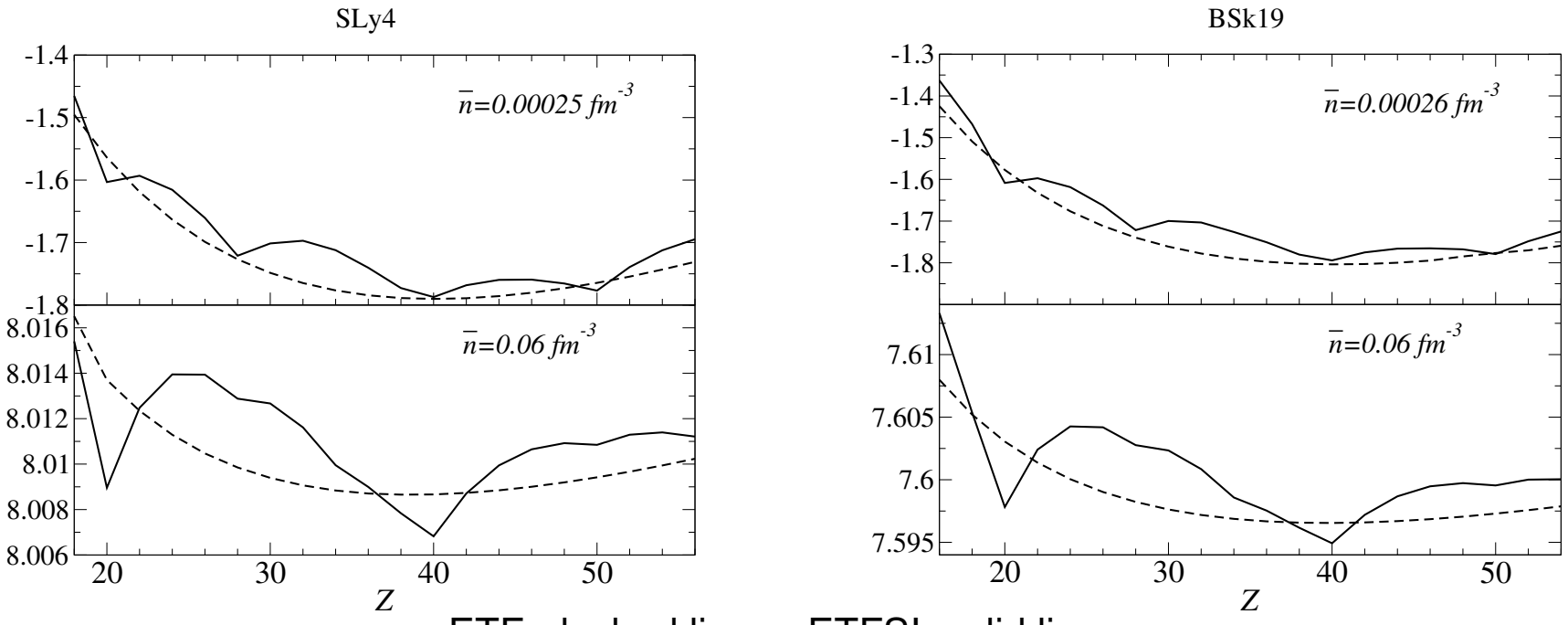

ETF: dashed lines - ETFSI: solid lines

Composition of the inner crust of a nonaccreting neutron star: proton pairing

Impact of proton pairing (BCS approximation) with BSk21.

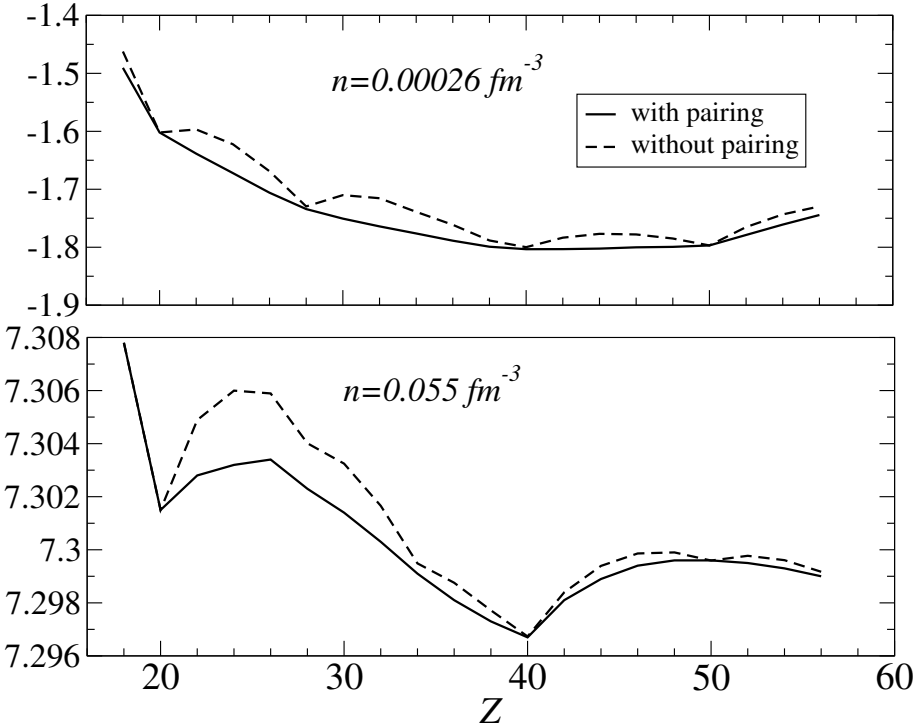

At low densities, $Z = 42$ is energetically favored, but by less than 5×10^{-4} MeV per nucleon.

A large range of values of Z is expected in a real neutron star.

Pearson,Chamel,Pastore,Goriely,Phys.Rev.C91, 018801 (2015).

Role of neutron superfluidity on the neutron specific heat with BSk21:
Pastore, Phys.Rev.C91,015809 (2015).
Generic interpolating formula valid for any temperature:
Pastore, Chamel, Margueron, MNRAS 448, 1887 (2015).

Conclusions&Perspectives

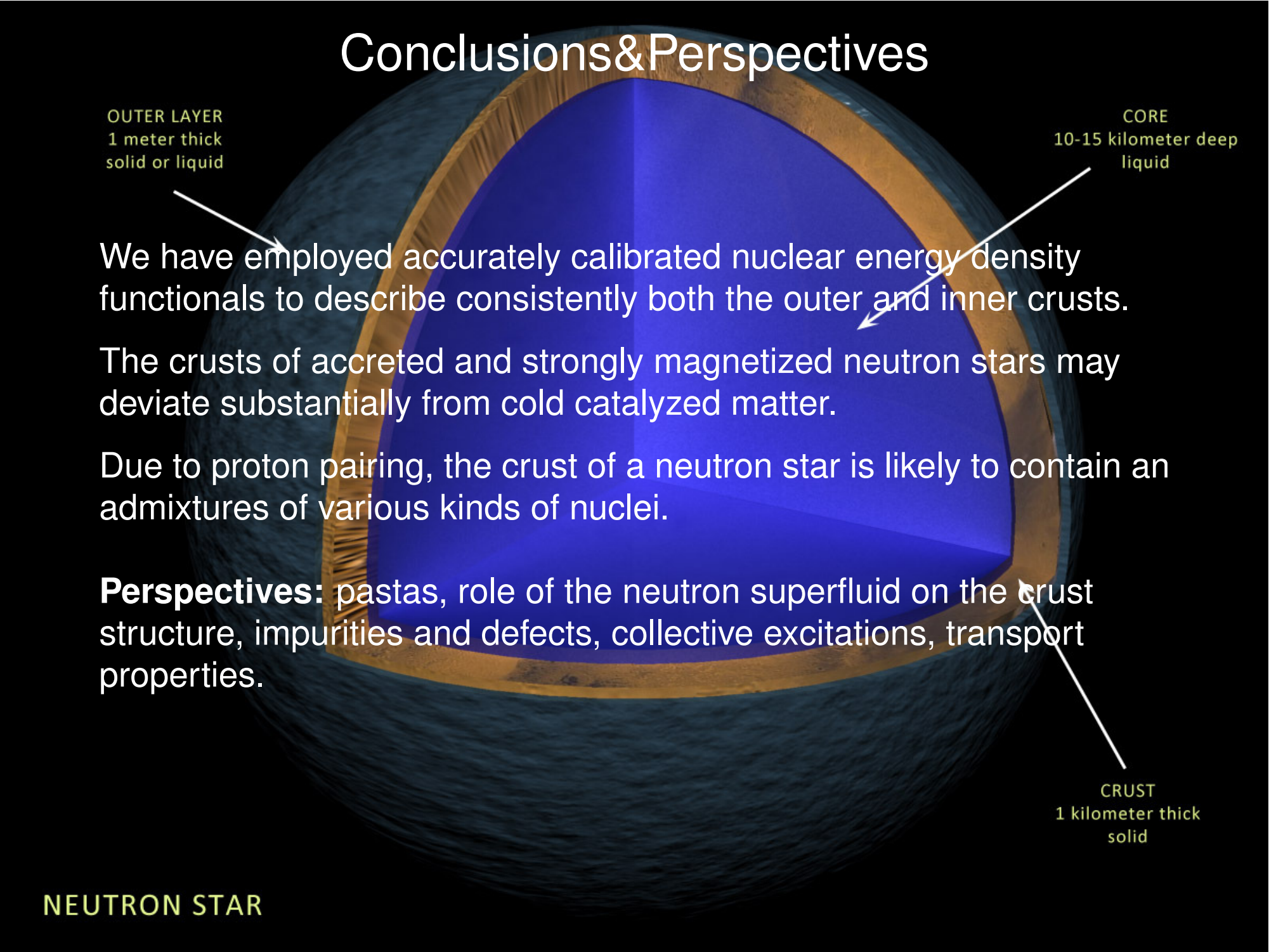

We have employed accurately calibrated nuclear energy density functionals to describe consistently both the outer and inner crusts.

The crusts of accreted and strongly magnetized neutron stars may deviate substantially from cold catalyzed matter.

Due to proton pairing, the crust of a neutron star is likely to contain an admixtures of various kinds of nuclei.

Perspectives: pastas, role of the neutron superfluid on the crust structure, impurities and defects, collective excitations, transport properties.